Neutrino emission from neutron star matter

Omar Benhar[†] and Lucas Tonetto[‡]

INFN, Sezione di Roma
Dipartimento di Fisica, Sapienza Università di Roma
I-00185 Roma, Italy
[†]*omar.benhar@roma1.infn.it*
[‡]*lucas.tonetto@uniroma1.it*

The temperature of a newly formed neutron star is believed to be as high as 10^{11} K, corresponding to a thermal energy of about 10 MeV. After a time $t \sim 50$ s, the neutrino mean free path in nuclear matter exceeds the typical star radius, R $\sim$ 10 Km, and neutrino emission becomes the dominant mechanism of energy loss, eventually bringing the temperature down to $\sim 10^8$ K. Neutrinos also play a critical role in determining the composition of matter in the star interior, consisting primarily of a charge-neutral mixture of neutrons, protons and leptons in β-equilibrium. This article provides an introduction to the weak interactions of nucleons in nuclear matter, as well as a concise review of the neutrino emission reactions taking place in the neutron star core. The approximations involved in the standard theoretical treatment of thermal and dynamical effects are analysed in the light of the recent progress of the field, and the prospects for future developments are outlined.

Keywords: neutrino emission, nuclear matter, neutron stars

PACS numbers:25.30.Pt,13.15.+g,26.60.-c,24.10.Cn

1. Introduction

The development of a consistent theoretical framework for the description of neutrino emission and propagation in dense matter is a prerequisite for large-scale simulations of a number of astrophysical processes, including supernova explosions, neutron star cooling, and binary neutron star mergers; see, e.g., Refs. [1, 2].

Neutrinos are a primary factor in the thermal evolution of neutron stars, and are critical for the determination of matter composition in the star interior [3, 4]. A prominent role is played by the neutrino emission processes taking place in the neutron star core, which is believed to consist predominantly of a charge-neutral fluid of neutrons, protons and leptons in weak equilibrium.

Although the fundamental theories of strong and weak interactions predict the appearance of different forms of matter—such as strange baryonic matter or quark matter—in the high-density limit, the validity of the description in terms of nucleons

is strongly supported by Bayesian inference analyses of recent astronomical data [5, 6]. The results of these studies indicate that a phase transition is, in fact, unlikely to occur even in the most massive neutron star observed so far [7], the central density of which exceeds the density of atomic nuclei by a factor of ~ 5. As recently pointed out by the authors of Ref. [5], independent experimental evidence reinforcing this conclusion is provided by the emergence of y-scaling in electron-nucleus scattering data; see Ref. [8] and references therein.

Neutrinos are also emitted from the low-density matter comprising the neutron star crust through a variety of reasction mechanisms. However, a discussion of these processes—which are known to be important, and must be taken into account in numerical studies of neutron star cooling—is outside the scope of our work. The interested reader is referred to the exhaustive reviews of Yakovlev *et al.* [9] and Chamel and Haensel [10].

It is important to realise that, in spite of the fact that neutrino-nucleon interactions in free space can be understood within the framework of the standard model of particle physics, the description of weak interactions in nuclear matter involves a host of challenging issues, originating mainly from the complexity of nuclear structure and dynamics. Additional difficulties arise from the treatment of thermal effects in protoneutron stars and in the remnants of neutron star mergers, the temperatures of which lie in the tens of MeV range.

The simplest reactions leading to neutrino and antineutrino emission from nuclear matter, referred to as Urca processes, are neutron β-decay and the capture of the associated charged lepton by a proton. Early analyses of these processes—involving a number of simplifying assumptions expected to be applicable in the low-temperature regime—revealed that the requirement of momentum conservation leads the emergence of a lower bound for the proton density. This result has important implications because, depending on the nuclear matter equation of state, the appearance of the threshold may prevent activation of the Urca processes in most neutron stars.

In the absence of Urca processes, the dominant neutrino and antineutrino emission reactions, dubbed modified Urca, proceed through a mechanism in which momentum conservation is enabled by the presence of an additional nucleon, acting as a spectator. As a consequence, the calculation of the corresponding rates requires a model of the nucleon-nucleon interaction. In their groundbreaking work of the late 1970s [11], Friman and Maxwell employed a number of low-temperature approximations and a simplified model of nuclear dynamics, based on the one-pion-exchange potential. The results of the analysis of Ref. [11]—which was pursued further and generalised by the authors of Refs. [9,12]—provided the baseline for later theoretical studies of the modified Urca process.

A significantly improved description of nuclear dynamics—involving the use of a realistic Hamiltonian and the G-matrix formalism—was employed by Shternin *et al.* to obtain the modified Urca reaction rates reported in Ref. [13]. This work can be

seen as a pioneering attempt to study neutrino emission from nuclear matter using a realistic nuclear Hamoltonian and the formalism of nuclear many-body theory.

Recently, significant efforts have been made to go beyond the approximations involved in the work of Friman and Maxwell [14–18]. These studies, featuring both a detailed treatment of thermal effects and a more realistic description of nuclear dynamics, were strongly motivated by the advent of multimessenger astronomy, and the ensuing unprecedented progress of neutron star observations; see, e.g., Ref. [19].

Ideally, neutrino emission from neutron stars should be described within a unified framework, in which the impact of temperature and nuclear dynamics on all relevant nuclear matter properties—from the equation of state, to the nucleon effective masses and chemical potentials—are consistently taken into account. Such an approach has been pursued by the authors of Refs. [17,18], who employed an effective Hamiltonian derived from state-of-the-art phenomenological potentials [20], and the formalism for the treatment of hot nuclear matter discussed in Refs. [21,22].

This article is intended to provide a concise description of the main processes leading to neutrino emission from nuclear matter, as well as a review of the results of selected theoretical approaches employed for their study. The remainder of the manuscript is organised as follows. After a brief introduction to the weak interactions of isolated nucleons, Sect. 2 analyses the corresponding processes in nuclear matter, with an emphasis on the impact of nuclear dynamics beyond the mean-field approximation. Section 3 is devoted to the discussion of the Urca and modified Urca reactions, and to a description of the theoretical models employed to obtain the corresponding neutrino emission rates. Finally, the concluding section summarises the present status of the field and lays down the prospects of future developments.

2. Weak interactions in nuclear matter

In the energy regime relevant to neutron star physics, weak interactions involving leptons and baryons can be accurately described replacing the exchange of the gauge bosons $W^\pm$ and Z_0—the masses of which are ~ 80 and ~ 90 GeV, respectively—with a contact four-fermion interaction. This tenet lies at the basis of the celebrated Fermi theory of neutron β-decay.

2.1. *Nucleon weak interactions in free space*

The Fermi Lagrangian describing charged-current (CC) and neutral-current (NC) nucleon weak interactions—associated with $W^\pm$ and Z_0 exchange, respectively—can be written as a current-current product in the form

$$\mathcal{L}_F(x) = -\frac{G_w}{\sqrt{2}} \, \ell_\alpha(x) j^\alpha(x) \quad , \qquad G_w = \begin{cases} G_F & (NC) \\ G_F \cos\theta_C & (CC) \end{cases} , \qquad (1)$$

with $G_F = 1.166 \times 10^{-5}$ GeV^{-2} and $\theta_C = 13.02°$ being the Fermi coupling constant and the Cabibbo mixing angle, respectively. The explicit expressions of the lepton

4 *O. Benhar & L. Tonetto*

currents, $\ell_\alpha(x)$, are

$$\ell_\alpha(x) = \begin{cases} \overline{\psi}_\ell(x)\gamma_\alpha(1 - \gamma_5)\psi_\nu(x) & (CC) \\ \overline{\psi}_\nu(x)\gamma_\alpha(1 - \gamma_5)\psi_\nu(x) & (NC) \end{cases} \quad , \tag{2}$$

with ψ_ν and ψ_ℓ being the Dirac fields describing a neutrino and the associated charged lepton. The nucleon currents can be conveniently written in the form

$$j^\alpha(x) = \begin{cases} \overline{\Psi}_N(x)\gamma^\alpha(g_V - g_A\gamma_5)\tau^\pm\Psi_N(x) & (CC) \\ \overline{\Psi}_N(x)\frac{1}{2}\gamma^\alpha(c_V - c_A\gamma_5)\Psi_N(x) & (NC) \end{cases} \quad , \tag{3}$$

where g_V and g_A (c_V and c_A) are the CC (NC) vector and axial-vector neutrino-nucleon coupling constants. The nucleon field Ψ_N is an isospin doublet, the upper and lower components of which are the proton and neutron fields ψ_p, and ψ_n, while $\tau^\pm$ denotes the isospin raising and lowering operators, associated with $W^\mp$ exchange, respectively.

Neutral current interactions in nuclear matter have been discussed extensively in studies of neutrino-pair bremsstrahlung, as well as in investigations of reactions involving more exotic particles, such as axions; see, e.g., Refs. [23,24]. This paper, on the other hand, is limited to a discussion of charged current interactions, which are known to provide the dominant contribution to neutrino and antineutrino emission from neutron stars.

In the non relativistic limit, routinely employed to describe the nucleon, the upper line of the right-hand side of Eq. (3) is replaced by

$$j^{\pm\alpha} \equiv (j^{\pm0}, \mathbf{j}^\pm) \quad , \text{ with } \quad \begin{cases} j^{\pm0} = g_V \, e^{i\mathbf{q}\cdot\mathbf{x}} \, \tau^\pm \\ \\ \mathbf{j}^\pm = g_A \, e^{i\mathbf{q}\cdot\mathbf{x}} \, \boldsymbol{\sigma} \, \tau^\pm \end{cases} \quad , \tag{4}$$

where $\boldsymbol{\sigma} \equiv (\sigma_1, \sigma_2, \sigma_3)$, with the σ_i's being Pauli matrices, describes the nucleon spin, while $\mathbf{q}$ denotes the momentum transfer to the nucleon.

2.2. *Weak interactions in matter and nuclear dynamics*

Theoretical studies of CC weak interaction processes in nuclear matter involve the evaluation of transition amplitudes that can be written in the form

$$M_{0F}^\alpha = \langle F| \, J^{+\alpha} \, |0\rangle \, , \tag{5}$$

with

$$J^{+\alpha} = \sum_{i=1}^{A} j_i^{+\alpha} \, , \tag{6}$$

where $j_i^{+\alpha}$ is the current operator acting on the i-th nucleon and A is the number of nucleons*. For any proton and neutron densities ϱ_p and ϱ_n, the initial and final

---

*In nuclear matter, both A and the normalisation volume V tend to infinity, with the baryon number density $\varrho_B = A/V$ remaining finite.

states of Eq. (5) are solutions of the many-body Schrödinger equations

$$ \mathrm{H}|0\rangle = E_0|0\rangle \qquad , \qquad \mathrm{H}|F\rangle = E_F|F\rangle \ , \tag{7} $$

with

$$ \mathrm{H} = \sum_{i=1}^{A} \frac{\mathbf{k}_i^2}{2m_N} + \sum_{j>i=1}^{A} v_{ij} + \sum_{k>j>i=1}^{A} V_{ijk} \ . \tag{8} $$

Here, m is the nucleon mass, $\mathbf{k}_i$ denotes the momentum of the i-th nucleon, and the potentials v_{ij} and V_{ijk} describe nucleon-nucleon (NN) and irreducible three-nucleon (NNN) interactions, respectively. Advanced models of the Hamiltonian provide a quantitative account of the observed properties of the two- and three-nucleon systems—which are calculable to high accuracy—and are well suited to explain the equilibrium properties of isospin-symmetric matter inferred from nuclear systematics. It should be pointed out that the basic assumption underlying the treatment of hot matter within nuclear many-body theory is that at low-to-moderate temperatures—typically $T \ll m_\pi$, $m_\pi \approx 140$ MeV being the pion mass—nuclear dynamics, as described by the Hamiltonian of Eq. (8), is largely unaffected by thermal effects.

Owing to the strong spin-isospin dependence of the potentials appearing in Eq. (8), the solution of the Schrödinger equation using non perturbative methods—notably those based on Quantum Monte Carlo techniques [25]—is out of reach of the present computing capabilities for nuclei having $A \geq 12$. On the other hand, the use of standard perturbation theory is hampered by the strongly repulsive nature of short-range NN interactions, which makes the matrix elements of v_{ij} too large for a perturbative expansion to converge. As a consequence, the evaluation of the nuclear transition amplitude of Eq. (5) unavoidably requires the introduction of simplifying assumptions.

2.2.1. *The mean-field approximation*

The mean-field approximation (MFA)—underlying the nuclear shell model—is based on the tenet that nucleons can be treated as independent particles subject to an average potential U_N, with $N = n, p$, similar to the quasiparticles of Landau's theory of normal Fermi liquids [26]. Within this scheme, the lowest-energy state of nuclear matter at temperature T, baryon number density ϱ_B and proton fraction $x_p = \varrho_p/\varrho_B$ can be written in terms of eigenstates of the mean-field Hamiltonian belonging to the eigenvalues

$$ e_N(k) = \frac{\mathbf{k^2}}{2m} + U_N(k) \ , \tag{9} $$

with $k = |\mathbf{k}|$, distributed according to the Fermi-Dirac function

$$ n_N(k,T) = \left\{ 1 + \mathrm{e}^{[e_N(k)-\mu_N]/T} \right\}^{-1} \ . \tag{10} $$

The above equation describes the probability of finding a nucleon of species N in the state specified by momentum $\mathbf{k}$, the energy of which, $e_N(k)$, is given by Eq. (9). The chemical potential μ_N is determined by the constraint

$$\frac{2}{V} \sum_{\mathbf{k}} n_N(k, T) = \varrho_N \ , \tag{11}$$

where V is the normalisation volume, and the factor 2 accounts for the spin degeneracy of momentum eigenstates. It follows that, in general, μ_N depends on T and the particle number density ϱ_N.

Because the nuclear weak current defined by Eq. (6) is the sum of single-nucleon operators, in order for the transition amplitude M_{0F}^α not to vanish, the MFA initial and final states can only differ by one orbital. Therefore, $|F\rangle$ is obtained from the ground state by replacing a neutron of momentum $\mathbf{k}_n$, distributed according to $n_n(k_n, T)$, with a proton, the momentum of which, $\mathbf{k}_p$, follows the distribution $1 - n_p(k_p, T)$. The energies and momenta of the states $|F\rangle$ and $|0\rangle$ are trivially related through $E_F = E_0 - e_n(k_n) + e_p(k_p)$, and $\mathbf{P}_F = \mathbf{P}_0 - \mathbf{k}_n + \mathbf{k}_p$, respectively.

Note that, in the $T \to 0$ limit, $n_N(k, T) \to \theta[\mu_N - e_N(k)]$, with $\theta(x)$ being the Heaviside step function, and $\mu_N \to e_{F_N}$. Here, the Fermi energy is defined as $e_{F_N} = e_N(k_{F_N})$, with the Fermi momentum k_{F_N} being related to the corresponding number density through $k_{F_N} = (3\pi^2 \varrho_N)^{1/3}$. The resulting $T = 0$ ground state consistes of neutrons and protons occupying all energy levels corresponding to momenta such that $k_n < k_{F_n}$ and $k_p < k_{F_p}$, while $|F\rangle$ is a one-particle–one-hole state, in which a neutron with $k_n < k_{F_n}$ is replaced by a proton with $k_p > k_{F_p}$.

2.2.2. *Nuclear dynamics beyond the mean field and short-range correlations*

While being able to explain a number of important properties of atomic nuclei, the MFA is inherently incomplete, in that it fails to take into account the effects of short-range correlations (SRC) among the nucleons, originating mainly from strongly repulsive nuclear forces. The most prominent signature of SRC is the appearance of high-momentum nucleons in the aftermath of virtual NN scattering processes, associated with a suppression of the probability of finding two nucleons within the range of the repulsive interactions. In Nuclear Many-Body Theory (NMBT), this *screening* effect is effectively accounted for through a *renormalisation* of the NN potential of Eq. (8), leading to the determination of a density-dependent *effective interaction*, suitable to carry out perturbative calculations of nuclear matter properties.

Unambiguous evidence of correlation effects in nuclei—first observed in a series of pioneering studies of electron-induced proton knockout reactions, concisely reviewed in Ref. [27]—has been provided by a wealth of electron-nucleus scattering data, collected over many decades using a variety of targets; see, e.g., Refs. [28,29].

Two main approaches—outlined in, e.g., Ref. [30]—have been followed to tame the non perturbative nature of the NN interaction. The first one is based on the

replacement of the bare v_{ij} with the well-behaved operator describing NN scattering in the nuclear medium. This effective interaction, referred to as G-matrix, can be used in perturbation theory in conjunction with the basis of eigenstates of the non interacting system. In the alternative approach, on the other hand, the NN potential v_{ij} is kept unchanged, while the Fermi gas basis is replaced with a complete set of states embodying the screening effect originating from SRC.

The *correlated* ground state, $|0\rangle$, is obtained from the transformation

$$|0\rangle = \frac{\mathcal{F}\,|0)}{\sqrt{(0|\mathcal{F}^\dagger\mathcal{F}|0)}}\ ,\tag{12}$$

where $|0)$ denotes the Fermi gas ground state and

$$\mathcal{F} = \left\{ \mathcal{S} \prod_{j>i=1}^{A} f_{ij} \right\}\ ,\tag{13}$$

with the operator structure of the NN *correlation functions* f_{ij} reflecting the spin-isospin dependence of the potential v_{ij}. Note that, in view of the fact that $[f_{ij}, f_{jk}] \neq 0$, the product appearing in the right-hand side of the above equation needs to be symmetrised through the action of the operator $\mathcal{S}$.

The radial dependence of the correlation functions is obtained by solving a set of Euler-Lagrange equations resulting from functional minimisation of the expectation value of the Hamiltonian of Eq. (8) in the correlated ground state of nuclear matter at $T = 0$. The choice of determining the correlation functions in cold matter is supported by the results of numerical calculations at $T \neq 0$, showing that the temperature dependence of f_{ij} remains negligibly small for temperatures as high as ~ 20 MeV.

In the wake of the pioneering work of Cowell and Pandharipande [31], the correlated ground state defined by Eqs. (12) and (13) has been employed to define a density-dependent effective interaction, denoted $\widetilde{v}_{ij}$, through the relation

$$\langle 0|\mathrm{H}|0\rangle = (0|\left\{ \sum_{i=1}^{A} \frac{\mathbf{k}_i^2}{2m} + \sum_{j>i=1}^{A} \widetilde{v}_{ij} \right\}|0)\ ,\tag{14}$$

with H being the nuclear Hamiltonian of Eq. (8). For any fixed nucleon density ϱ_B, $\widetilde{v}_{ij}$ is obtained by applying the cluster expansion technique, thoroughly described in Ref. [32], which amounts to rewrite the left-hand side of the above equation as a sum of contributions arising from subsystems, or clusters, involving an increasing number of nucleons; a detailed discussion of the determination of $\widetilde{v}_{ij}$ from a nuclear Hamiltonian involving both NN and NNN potentials can be found in Refs. [20, 21].

The resulting effective interaction is independent of temperature by construction, and designed to reproduce the ground-state energies of cold isospin-symmetric nuclear matter (SNM) and pure neutron matter (PNM) obtained using advanced computational approaches, such as the Auxiliary Field Diffusion Monte Carlo (AFDMC) method or the variational scheme known as Fermi Hyper-Netted

Chain/Single Operator Chain (FHNC/SOC) summation. It should be pointed out that the formalism based on the effective interaction $\widetilde{v}_{ij}$ allows for a consistent treatment of equilibrium and dynamical properties of nuclear matter within a unified framework. A notable early application was the calculation of the shear viscosity and thermal conductivity of PNM described in Refs. [33, 34]. In addition, $\widetilde{v}_{ij}$ can be used to derive the mean field U_N from the nuclear Hamiltonian of Eq. (8). In the Hartree-Fock approximation, the resulting expression turns out to be

$$U_N(k) = \sum_{\mathbf{k}'} (\mathbf{k}\mathbf{k}'| \sum_{j>i=1}^{A} \widetilde{v}_{ij} \, |\mathbf{k}\mathbf{k}'\rangle_A \; n_N(k', T) \; , \tag{15}$$

where n_N is the Fermi-Dirac distribution of Eq. (10), and $|\mathbf{k}\mathbf{k}'\rangle_A = |\mathbf{k}\mathbf{k}'\rangle - |\mathbf{k}'\mathbf{k}\rangle$ denotes the antisymmetric state of two non-interacting nucleons.

2.3. *Effective weak current*

The correlation operator $\mathcal{F}$ of Eq. (13) is also employed to obtain the complete set of states referred to as correlated basis functions, or CBF, defined as

$$|n\rangle = \frac{\mathcal{F} \, |n)}{\sqrt{(n|\mathcal{F}^\dagger \mathcal{F}|n)}} \; , \tag{16}$$

where $|n)$ denotes an excited state of the non-interacting Fermi gas. The set $\{|n\rangle\}$ is suitable to perform calculations of the nuclear transition amplitudes of Eq. (5) including the effects of SRC; for a concise review of the application of the CBF formalism to nuclear matter, see, e.g., Ref. [30].

It should be kept in mind that, within the independent-particle model, the structure of the nuclear matter eigenstates appearing in Eq. (5) is dictated only by translation invariance and Fermi-Dirac statistics. As a consequence, the transition amplitude M_{0F}^α obtained from the Fermi gas model is left unchanged by the inclusion of nuclear dynamics at mean-field level. On the other hand, the results of a number of theoretical studies provide convincing evidence that SRC lead to a sizeable suppression of weak interactions in nuclear matter; see, e.g., Refs. [35–38].

These findings can be understood considering that the same mechanism accounted for by renormalisation of the nuclear Hamiltonian—that is, the appearance of high-momentum nucleons and the ensuing depletion of the Fermi gas eigenstates—also leads to a quenching of the transition amplitude of Eq.(5), which can likewise be described in terms of a *renormalised current operator* and Fermi gas states.

Within the approach based on the CBF formalism, the effective weak current $\widetilde{j}_i^+$ is defined by the equation

$$\langle F|J^{+^\alpha}|0\rangle = (F| \sum_{i=1}^{A} \widetilde{j}_i^{+^\alpha}|0) \; , \tag{17}$$
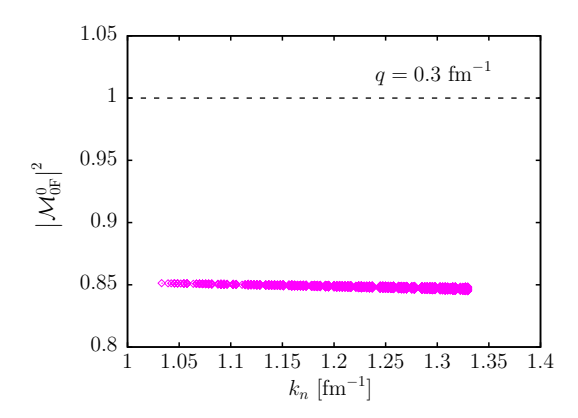
Fig. 1. Squared transition matrix element of the $\alpha = 0$ component of the effective weak current, defined by Eq. (17), in cold SNM at equilibrium density. The results, corresponding to fixed momentum transfer $q = 0.3$ fm^{-1}, are displayed as a function of the neutron momentum. For comparison, the dashed horizontal line shows the predictions of the independent-particle model. Adapted from Ref. [36].

to be compared to Eq. (14). The derivation of the effective current $\widetilde{j}_i^+$ from the above equation, based on the cluster expansion technique, is discussed in Ref. [38].

As an example, Fig. 1 shows the squared transition matrix element of the $\alpha = 0$ component of the effective weak current, defined according to Eq. (17), in isospin-symmetric nuclear matter at equilibrium density, $\varrho_0 = 0.16$ fm^{-3}, and $T = 0$. The calculation was performed by the authors of Ref. [36], using the CBF formalism and correlation functions obtained from a realistic nuclear Hamiltonian including NN and NNN interactions. The results, corresponding to fixed momentum transfer $q = |\mathbf{k}_p - \mathbf{k}_n| = 0.3$ fm^{-1}, show that the inclusion of SRC leads to a significant departure from the predictions of the independent-particle model—represented by the dashed horizontal line—largely independent of the magnitude of the neutron momentum.

3. Neutrino emission mechanisms

This paper is limited to a discussion of neutrino and antineutrino emission from charge-neutral and β-stable matter consisting of neutrons, protons and electrons, the densities of which are denoted ϱ_n, ϱ_p, and ϱ_e, respectively. In such a system, referred to as *npe* matter, electrons are treated as ultra relativistic non interacting particles, while interactions among the nucleons are described within the non relativistic framework outlined above. Neutrinos and antineutrinos are assumed to stream freely through matter, with their densities and chemical potentials being therefore vanishing. The extension of the formalism to take into account the appearance of muons—which is energetically favoured when the electron chemical potential exceeds the muon rest mass—does not involve any conceptual issues.

In principle, the microscopic description of nuclear matter should take into ac-

count possible deviations from the Fermi liquid behaviour associatd with the appearance of superfluid and superconducting phases [39], as well as with the onset of pion condensation [40]. However, although the emergence of these non standard forms of nuclear matter may affect neutrino emission and neutron star cooling—see, e.g., Refs. [41–43]—their discussion is beyond the scope of the present work.

3.1. *Direct Urca processes*

The simplest weak interaction processes leading to ν and $\bar{\nu}$ emission from *npe* matter are neutron β-decay and the inverse electron capture reaction

$$n \to p + e + \bar{\nu} \quad , \quad p + e \to n + \nu \ . \tag{18}$$

The above reactions—first discussed by Gamow and Schoenberg in the 1940s [44], and famously named Urca processes [45]—provide the most effective cooling mechanism of massive neutron stars; see, e.g., Ref. [41]. In view of the discussion of the more complex neutrino emission mechanism to be discussed in Sect. 3.3, hereafter the processes (18) will be referred to as direct Urca, or dUrca.

At equilibrium, neutron decay and electron capture contribute equally to the neutrino emissivity—defined as the total ν and $\bar{\nu}$ energy emitted per unit time and volume—and the chemical potentials of the degenerate fermions satisfy the condition

$$\mu_n = \mu_p + \mu_e \ . \tag{19}$$

The solution of equation (19) yields the equilibrium value of the proton fraction $x_p = \varrho_p/\varrho_B$, which fully determines matter composition at fixed T and ϱ_B.
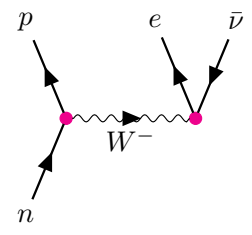

Fig. 2. Diagrammatic representation of $\bar{\nu}$ emission through the dUrca process in *npe* matter.

For illustration, let us consider $\bar{\nu}$ emission associated with the elementary process illustrated by the diagram of Fig. 2. The corresponding transition rate can be obtained using Feynman diagram techniques, keeping in mind that the external nucleon lines and the vertices *do not* represent non interacting fermions and their

weak interactions in free space. The resulting expression can be cast in the form

$$W_U = \frac{(G_F \cos \theta)^2}{2} \frac{1}{4 E_e E_\nu} L_{\alpha\beta} S^{\alpha\beta} \ , \tag{20}$$

where the tensor $L^{\alpha\beta}$ can be readily written in terms of the lepton four-momenta, $k_e \equiv (E_e, \mathbf{k_e})$ and $k_\nu \equiv (E_\nu, \mathbf{k}_\nu)$, as

$$L_{\alpha\beta} = 8 \left[k_{e\alpha} k_{\nu\beta} + k_{e\beta} k_{\nu\alpha} - g_{\alpha\beta}(k_e k_\nu) + i \epsilon_{\alpha\beta\rho\sigma} k_e^\rho k_\nu^\sigma \right] \ , \tag{21}$$

with $g_{\alpha\beta} = \mathrm{diag}(1, -1, -1, -1)$ and $\epsilon_{\alpha\beta\rho\sigma}$ being the metric tensor and the four-dimensional Levi-Civita tensor, respectively.

The expression of $S^{\alpha\beta}$, involving the transition matrix elements of the nucleon weak current M_{0F}^α defined by Eq. (5), reads

$$S^{\alpha\beta} = \sum_F M_{0F}^{\alpha\,\dagger} M_{0F}^\beta \ (2\pi)^4 \delta^{(4)}(P_0 - P_F - k_e - k_\nu) \ , \tag{22}$$

where $P_0 \equiv (E_0, \mathbf{P}_0)$ and $P_F \equiv (E_F, \mathbf{P}_F)$ denote the four-momenta of the nuclear matter initial and final states. Within the independent particle model underlying the MFA, $S^{\alpha\beta}$ turns out to be diagonal, and the transition rate of the dUrca process—a pedagogical derivation of which can be found in, e.g., Ref [46]—reduces to

$$W_U = 2(G_F \cos \theta_C)^2 \left[g_V^2 (1 + \cos \theta) + g_A^2 (3 - \cos \theta) \right] \tag{23}$$
$$\times (2\pi)^4 \delta (E_n - E_p - E_e - E_\nu) \, \delta^{(3)} (\mathbf{k}_n - \mathbf{k}_p - \mathbf{k}_e - \mathbf{k}_\nu) \ ,$$

where $k_N \equiv (E_N, \mathbf{k}_N)$ denotes a nucleon four-momenta, $E_n = e_n(k_n)$, $E_p = e_p(k_p)$, and θ is the angle between the lepton momenta $\mathbf{k}_e$ and $\mathbf{k}_\nu$.

In the low-temperature regime relevant to neutron stars, all fermions participating in the dUrca processes are strongly degenerate, their momenta being close to the corresponding Fermi momenta. Under these conditions, the widely used Fermi surface approximation (FSA), which amounts to setting $|\mathbf{k}_i| = k_{F_i}$ with $i = n, p, e$, is expected to be reliably applicable. Assuming, in addition, that the neutrino momentum—the typical magnitude of which is $|\mathbf{k}_\nu| \sim T$—can be neglected with respect to the nucleon and electron Fermi momenta, the equation expressing momentum conservation can be written in the form

$$\mathbf{k}_n = \mathbf{k}_p + \mathbf{k}_e \ , \tag{24}$$

which entails the inequality

$$k_{F_p} \geq k_{F_n} - k_{F_e} \ . \tag{25}$$

By combining the above result with the constraints associated with baryon number conservation and charge neutrality, implying $\varrho_p = \varrho_B - \varrho_n = \varrho_e$, one obtains the condition $x_p = \varrho_p / \varrho_B \geq x_{\mathrm{thr}} = 1/9$, to be satisfied by the proton fraction x_p in order for the dUrca mechanism to be active.

Given a model of the nuclear mean field U_N, which determines the chemical potentials through Eqs. (9)–(11), the equilibrium value of the proton fraction x_p

at temperature T and baryon density ϱ_B is obtained from the solution of Eq. (19). As an example, the left panel of Fig. 3 shows the density dependence of the proton fraction of charge-neutral, β-stable matter at temperatures in the range $T = 0 - 20$ MeV reported in Ref. [22]. The effective interaction employed in these studies was derived by the authors of Refs. [20,21] using the CBF formalism and a phenomenological nuclear Hamiltonian comprising the Argonne v_6' NN potential [47] and and the Urbana IX NNN potential [48,49]. Thermal effects turn out to be significant, and lead to a departure from the monotonic behaviour typical of cold matter for $T \geq 20$ MeV.

In the low-temperature regime, in which the proton fraction increases with ϱ_B, the appearance of the threshold x_{thr} entails the occurrence of a corresponding threshold density ϱ_{thr}, determined by the condition $(k_{F_p} + k_{F_e})/k_{F_n} = 1$. The results displayed in the right panel of Fig. 3—obtained from the zero-temperature proton fraction of the left panel—show that $\varrho_{\text{thr}} \approx 0.4$ fm^{-3}. This relatively low value, exceeding nuclear saturation density by a factor of about 2.5, suggests that the dUrca process may, in fact, be allowed in neutron stars with the canonical mass $M = 1.4 \ M_\odot$.
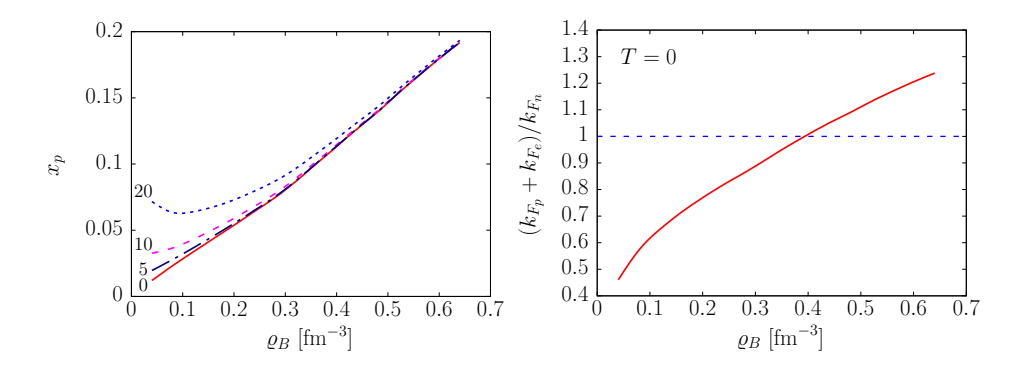

Fig. 3. Left panel: density dependence of the proton fraction in *npe* matter at temperature T =0, 5, 10, and 20 MeV. Adapted from Ref. [22]. Right panel: density dependence of the ratio $(k_{F_p} + k_{F_e})/k_{F_n}$. The horizontal line indicates the threshold for activation of the dUrca mechanism at $T = 0$. Reprinted from Ref. [17]. © Lucas Tonetto, 2024. All rights reserved.

It should be emphasised that the activation threshold of the Urca processes only appears in the limit of zero-temperature, which implies the onset of the strong degeneracy regime underlying the FSA. While laking a consistent interpretation at $T > 0$, however, the threshold obtained from the above procedure turns out to be useful as a baseline for the analysis of the T-dependence of *npe* matter composition; see, e.g., Ref. [50].

3.2. *Emissivity of the dUrca processes*

The neutrino emissivity associated with the dUrca processes is obtained from integration of the product between the reaction rate W_U, defined by Eqs. (20)-(22), and a factor describing the total phase space available to the participating particles, shaped by the Fermi-Dirac distributions. The resulting expression is

$$Q_U = 2 \int \, W_U \, E_\nu \, n_n(1 - n_p)(1 - n_e) \, \frac{d^3k_n}{(2\pi)^3} \frac{d^3k_p}{(2\pi)^3} \frac{d^3k_e}{(2\pi)^3} \frac{d^3k_\nu}{(2\pi)^3} \,, \qquad (26)$$

where the factor 2 is needed to include the contributions of both ν and $\overline{\nu}$.

3.2.1. *Low-temperature approximation*

In the low-temperature regime, the calculation of Q_U can be greatly simplified by neglecting $\mathbf{k}_\nu$ in the momentum-conserving δ-function, which allows to readily perform the $\cos\theta$ integration. In addition, the remaining integrations are routinely carried out by applying the so-called phase space decomposition [9], which amounts to substituting

$$\frac{d^3k_n}{(2\pi)^3} \frac{d^3k_p}{(2\pi)^3} \frac{d^3k_e}{(2\pi)^3} \longrightarrow \prod_{i=n,p,e} k_{Fi} m_i^* dE_i d\Omega_i \,, \qquad (27)$$

as prescribed by the FSA. Here, Ω_i is the solid angle specifying the direction of the momentum $\mathbf{k}_i$, and the fermion effective masses are defined as

$$\frac{1}{m_i^\star} = \frac{1}{k_{Fi}} \left(\frac{dE_i}{d|\mathbf{k}_i|} \right)_{|\mathbf{k}_i|=k_{Fi}} . \qquad (28)$$

Within the MFA, in which the reaction rate is given by Eq. (23), the resulting expression of the emissivity can be cast in the form [9]

$$Q_D \propto G_F^2 \cos^2\theta_c \, (1 + 3g_A^2) \, m_n^* \, m_p^* \, m_e^* \, T^6 \, \Theta_{npe} \,, \qquad (29)$$

with

$$\Theta_{npe} = \begin{cases} 1 & \text{if } k_{F_n} \leq k_{F_p} + k_{F_e} \\ 0 & \text{otherwise} \end{cases} , \qquad (30)$$

showing a specific power-law dependence on temperature—dictated by the number of degenerate fermions participating in the process—and the threshold behaviour as a function of proton fraction discussed above. Because both these features are determined by the use of the FSA, the occurrence of deviations from the predictions of Eq. (29)—which may originate from the failure of the low-temperature approximation as well as from effects of nuclear dynamics beyond the MFA—needs to be carefully analysed.

14   *O. Benhar & L. Tonetto*

3.2.2. *Thermal and correlation effects*

Figure 4 shows the density dependence of the emissivity of the Urca processes in *npe* matter at T = 0.1 MeV, evaluated within the approach based on the FSA and the phase space decomposition described above; the effective masses and chemical potentials of the degenerate fermions involved in the calculation of Q_U—derived from the CBF effective interaction defined by Eq. (14)—are thoroughly discussed in Ref. [22].
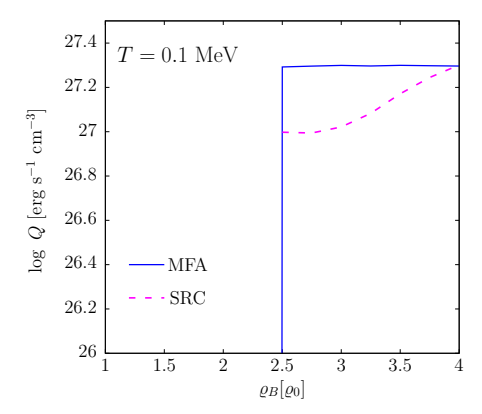

Fig. 4. Density dependence of the neutrino emissivity associated with the Urca processes in *npe* matter at $T = 0.1$ MeV, computed using the FSA and the phase space decomposition. The solid and dashed lines represent the results of obtained within the MFA ad including the effects of SRC, respectively. Note the activation threshold of the Urca processes at $\varrho = 2.5\ \varrho_0$. Reprinted from Ref. [17]. © Lucas Tonetto, 2024. All rights reserved.

The MFA predictions, represented by the solid line, are compared to the results obtained by replacing the free-space nucleon weak current, j_i^+, with the renormalised operator embodying the effects of SRC $\widetilde{j}_i^+$, defined by Eq. (17). The details of the derivation of $\widetilde{j}_i^+$ using the CBF formalism and the cluster expansion technique can be found in Ref. [17]. Is is apparent that the inclusion of nuclear dynamics beyond the MFA, while not affecting the occurrence of the threshold at $\varrho_{\rm thr} = 0.4\ {\rm fm}^{-3}$—consistent with the $T = 0$ result shown in the right panel of Fig. 3—leads to significant modifications of the density dependence of Q_U. The emissivity turns out to be reduced by as much as 50 % at $\varrho \approx \varrho_{\rm thr}$, and monotonically increases with ϱ. The MFA value is approached at $\varrho \approx 0.64\ {\rm fm}^{-3}$, corresponding to four times nuclear matter saturation density.

In order to shed light on the breakdown of the low-temperature approximation, the emissivities of the dUrca processes at temperature $T = 5$ and 10 MeV have been also evaluated lifting the simplifying assumptions implied in the FSA, and using Monte Carlo techniques to carry out the full phase space integrations involved in Eq. (26) [17]. The results of these calculations, displayed in the two panels of Fig. 5, clearly show that, owing to the thermal broadening of the Fermi surface, the sharp

threshold observed in Fig 4 is washed out already at $T = 5$ MeV. The emissivity turns out to be a smooth function of density over the whole range $1 \leq (\varrho_B/\varrho_0) \leq 4$, and approaches the predictions of the low-temperature approximation—shown by the thick solid line—with increasing ϱ_B. Note that at $T = 10$ MeV the asymptotic value is reached at larger density.
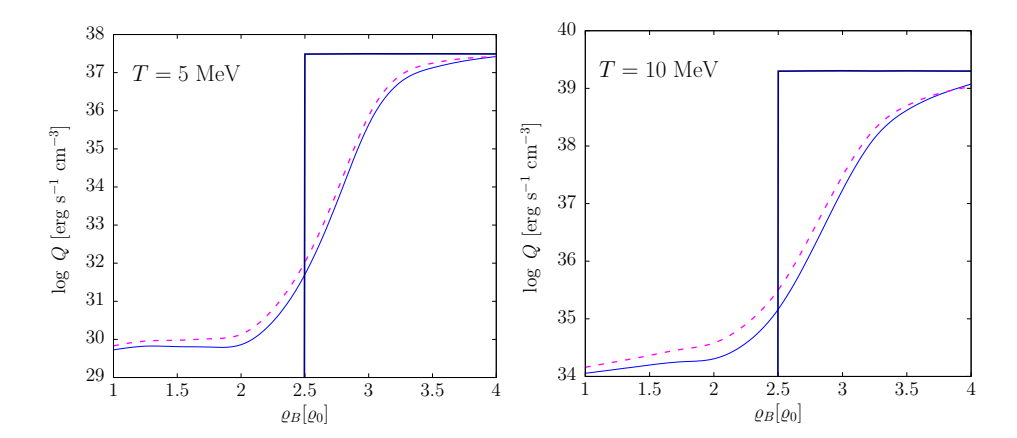

Fig. 5. Emissivity of the dUrca processes at $T = 5$ and 10 MeV, obtained from Eq. (26) without using the FSA, and carrying out the full phase space integration. The solid and dashed lines correspond to calculations performed with and without inclusion of the SRC, respectively. For comparison, the thick solid lines at $\varrho > 2.5 \, \varrho_0$ show the results obtained using the low-temperature approximations described in the text. Reprinted from Ref. [17]. © Lucas Tonetto, 2024. All rights reserved.

The solid and dashed lines of Fig. 5, corresponding to the emissivities obtained with and without inclusion of SRC—which will be denoted Q_U^{SRC} and Q_U^{MFA}, respectively—exhibit largely similar behaviours. The impact of SRC can be best identified considering the density dependence of the ratio Q_U^{SRC}/Q_U^{MFA}, displayed in Fig. 6 for both $T = 5$ and 10 MeV.

All in all, the picture emerging from Figs. 5 and 6 indicates that, regardless of the inclusion of correlation effects, releasing the low-temperature approximation leads to significant modifications of the emissivity at all densities. Note that the $\sim 50\%$ quenching of the ratio Q_U^{SRC}/Q_U^{MFA} occurring at $\varrho_B \approx 2.5 \, \varrho_0$, is reminiscent of the $T = 0.1$ MeV result of Fig. 4. The differences between the curves corresponding to different temperatures, observed Fig. 6 for large values of ϱ_B, can be understood considering the interplay between thermal and density-dependent dynamical effects on equilibrium and non-equilibrium properties of nuclear matter, discussed in Ref. [50].
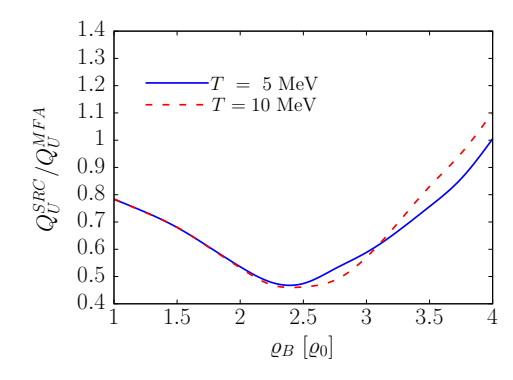
16   *O. Benhar & L. Tonetto*

Fig. 6. Density dependence of the ratio between the emissivities of the dUrca processes computed with and without inclusion of SRC at temperature $T = 5$ and 10 MeV. Adapted from Ref. [17].

3.3. *Modified Urca processes*

The modified Urca, or mUrca, processes

$$n + N \to p + e + \overline{\nu} + N \quad , \quad p + e + N \to n + \nu + N \ , \tag{31}$$

where $N = n, p$ labels the neutron and proton branch, respectively, involve combinations of ν and $\overline{\nu}$ emission through the dUrca reactions (18) and a NN collision; two examples of mUrca processes are illustrated by the diagrams of Fig. 7. Note that, owing to the presence of the NN interaction, the MFA is inherently inadequate to describe the mUrca mechanism.
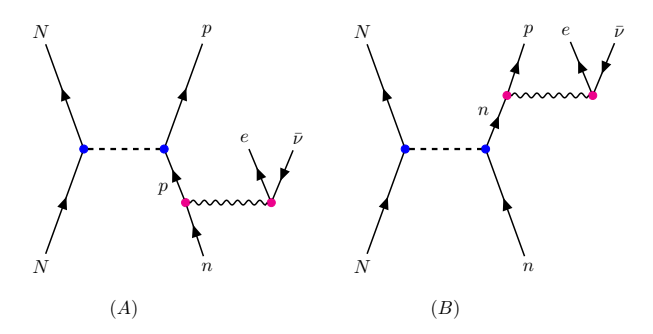

Fig. 7. Diagrammatic representation of $\overline{\nu}$ emission through modified Urca processes in *npe* matter. Both diagrams involve a combination of neutron β-decay and a NN interaction, depicted by the dashed line. The label $N = n, p$ corresponds to the neutron and proton branch, respectively.

It should be reminded that the dashed lines of Fig. (7) *do not* represent the NN potential v_{ij} appearing in the nuclear Hamiltonian of Eq.(8), which is not amenable to treatment by perturbation theory. In their seminal study of neutrino emissivities

associated with mUrca processes [11], Friman and Maxwell circumvented this problem using a simplified model of v_{ij}, comprising the long-range one-pion-exchange (OPE) interaction, supplemented by a short-range interaction parametrised according to the scheme of Landau's theory of Fermi liquids [26].

A comparison between Figs. 2 and 7 shows that, in addition to the dashed line representing the NN interaction, the diagrams depicting mUrca processes involve an internal fermion line, representing the nucleon propagator G_N. The authors of Ref. [11], whose results were obtained within the FSA described above and neglecting the momentum of the outgoing antineutrino, employed the approximate expression $G_N \approx 1/E_e$.

More detailed analyses of neutrino emission based on the conceptual framework underlying the work of Friman and Maxwell have been carried out by Yakovlev *et al.* [9, 12]. The results of these studies, illustrated in Fig. 8 for temperatures in the range $10^8 - 10^9$ K—corresponding to thermal energies $8.62 - 86.2$ keV—clearly show the threshold behaviour as a function of baryon density, expected in the $T \to 0$ limit. Note, however, that at densities close to the dUrca threshold, small deviations from the sharp discontinuity described by the step function of Eq. (30) are approximately taken into account by an exponential suppression of the emissivity. The effect of this correction is clearly visible at $T = 10^9$ K.

The dominant high-density component originates from the onset of the dUrca mechanism discussed in Sec. 3.2, while the much smaller sub-threshold contribution is associated with mUrca processes. The threshold values of matter density—$\varrho \gtrsim 1.2 \times 10^{15}$ g/cm^3, corresponding to baryon number densities $\varrho_B \gtrsim 0.72$ fm^{-3}, or $4.5 \, \varrho_0$—suggest that, according to the model employed by the authors, the dUrca process is only likely to be active in massive neutron stars, the central density of which exceeds the saturation density of SNM by a factor $4 - 5$.

An improved treatment of the neutrino emissivity originating from mUrca processes was proposed by Shternin *et al.* in Ref. [13]. In this work, the renormalised NN interaction was derived from a realistic nuclear Hamiltonian—comprising the Argonne v_{18} [51] NN potential and the UIX NNN potential [48, 49]—using the G-matrix formalism. The nucleon propagator was written in the quasiparticle form

$$G_N^{\mathrm{MFA}}(k, E) = \frac{1}{E - e_N(k)} \, , \tag{32}$$

with the nucleon energy of Eq. (9) computed in Brueckner Hartee-Fock approximation using Eqs. (9) and (15). The results reported in Ref. [13]—obtained by applying the FSA and the phase space decomposition—show that replacing the simplified interaction based on the OPE potential with the G-matrix in the calculation of the NN scattering amplitude results in a moderate decrease of the mUrca rate. On the other hand, the use of the nucleon propagator of Eq. (32) leads to a strong enhancement at all densities, and to the appearance of an unphysical divergence as the density approaches the activation threshold of the dUrca mechanism.

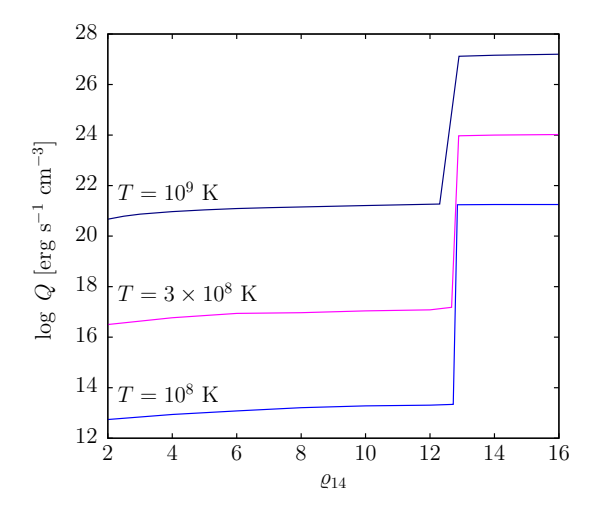The rate of the mUrca process was subsequently analysed by Suleiman *et al.* [14],

Fig. 8. Total neutrino emissivity in npe matter at $T = 10^8$, 3×10^8, and 10^9 K, displayed as a function of matter density measured in units of 10^{14} g cm^{-3}. Note that in these units the saturation density of cold nuclear matter is $\varrho_0 \approx 2.57$. The results have been obtained by Yakovlev *et al.* using the low-T approximation discussed in the text and the formalism based on the work of Friman and Maxwell [11]. Adapted from Ref. [9].

who carried out a detailed perturbative calculation based on the OPE interaction model, in which the treatment of thermal effects was improved by releasing the low-temperature approximations employed in Refs. [11,13]. Higher order dynamical effects were also taken into acount by assigning a finite lifetime, τ, to the quasiparticle states, and including lowest-order vertex corrections. According to this prescription, the single-nucleon energy acquires a constant imaginary part, $\Gamma = \tau^{-1}$, meant to parametrise the non vanishing width of the peaks appearing in the quasiparticle spectra. The most prominent effect of the broadening of the spectral lines in the finite-temperature formalism of Ref. [14] turns out to be the disappearance of the divergence observed by Shternin *et al.* [13].

3.4. *Recent developments*

Over the past couple of years, the dUrca and mUrca mechanisms, as well as their mutual relation, have been reexamined by the authors of Refs [15,16] using a relativistic formalism based on the polarisation tensor $\Pi^{\alpha\beta}$.

Within this approach, the neutrino emissivity is written in terms of the imaginary part of the contraction $L_{\alpha\beta}\Pi^{\alpha\beta}$—with $L_{\alpha\beta}$ being the lepton tensor of Eq. (21)—and the contributions of different reaction mechanisms can be consistently taken into account by using suitable definitions of $\Pi^{\alpha\beta}$.

In the loop approximation, schematically illustrated by the diagram of Fig. 9

(A), the polarisation tensor is defined as

$$\Pi^{\alpha\beta} = -i \int \frac{d^4p}{(2\pi)^4} \text{Tr}\big\{ j^{\alpha\dagger} G_p(p+q) j^\beta G_n(p) \big\} \ , \tag{33}$$

where j^α and $G_N(p)$ denote the nucleon weak current and the propagator of a relativistic nucleon with four-momentum p, the perturbative expansion of which is schematically depicted in the right panel of Fig. 9. A comparison with the diagrams of Figs. 2 and 7 reveals that diagrams (B) and (C), correspond to the dUrca and mUrca processes, respectively.

Within the loop approximation employed in Refs [15,16] the nucleon propagators include self-energy insertions, but vertex corrections are not taken into account. As a consequence, the Ward identities following from current conservation are not satisfied. This issue is known to be relevant in the analysis of nucleon interactions driven by the neutral weak current, the vector component of which is conserved. In the case of charged current interactions, on the other hand, the neutron-proton mass difference entails a violation of the Ward identities even in processes involving isolated nucleons.

As pointed out by the authors of Ref. [15], in nuclear matter the scale of the intrinsic violation of the Ward identities originating from isospin-symmetry breaking is dictated by the difference between the nucleon *effective* masses, which lies in the tens of MeV range. At $T \lesssim 10$ MeV, this difference turns out to be larger than the typical width of quasiparticle states employed in their study.
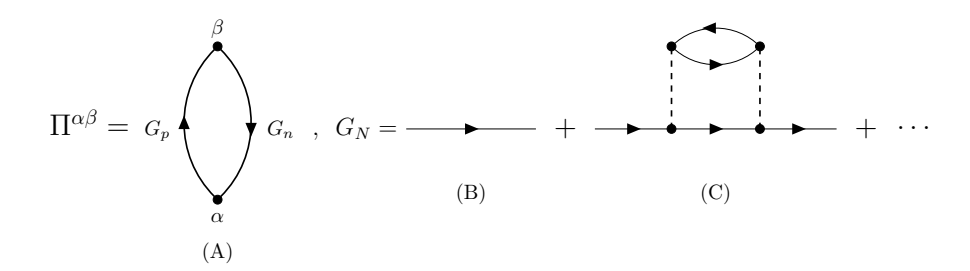

Fig. 9. Schematic representation of the polarisation tensor of Eq. (33), diagram (A), and lowest-order contributions to the nucleon propagator, diagrams (B) and (C).

Alford *et al.* [15] argued that the distinction between dUrca and mUrca reactions is somewhat artificial, and developed a systematic approach in which the corresponding contributions to the emissivity can be consistently taken into account within a unified framework. In the simplest implementation of this scheme—dubbed Nucleon Width Approximation, or NWA—the propagator of a nucleon with four

momrntum k is written in the form

$$G_N^{\text{NWA}}(k, m_N^\star, \Gamma_N) = \int_{-\infty}^{+\infty} dM \; G_N^{\text{MFA}}(k, M) R_N(M, \Gamma_N) \;, \qquad (34)$$

where $m_N^\star$ is the nucleon effective mass defined by Eq. (28), G_N^{MFA} denotes the relativistic generalisation of the MFA propagator of Eq. (32), and $R_N(M, \Gamma_N)$ is a Breit-Wigner distribution peaked at $M = m_N^\star$, whose width parametrises the collisional broadening of the quasiparticle spectral lines. This procedure allows one to obtain the *total* neutron decay rate from the dUrca contribution using

$$\Gamma^{\text{NWA}} = \int_{-\infty}^{+\infty} dM_n dM_p \; \Gamma^{\text{dUrca}}(M_n, M_p) R_n(M_n, \Gamma_n) R_p(M_p, \Gamma_p) \;. \qquad (35)$$

The results of Ref. [15], based on the so-called IUF model of the nuclear matter equation of state [52], are summarised in Fig. 10, in which the density dependence of the neutron decay rate at $T = 1$ MeV computed using the NWA is compared to the predictions of different approximation schemes. The curve labelled "no-prop mUrca" shows the baseline results of Friman and Maxwell [11], while the "mUrca with rel. prop." line has been obtained from a relativistic generalisation of the treatment of Ref. [13], and the long dashed line corresponds to the dUrca rate, computed carrying out the full phase space integration. The NWA calculation has been performed using the same nucleon width Γ—resulting from calculations carried out by the authors of Ref. [53] using the G-matrix formalism—for protons and neutrons. The emerging picture suggests a smooth transition from the low-density region, in which the emissivity is mainly driven by mUrca processes, to the high-density region, in which the dUrca mechanism is dominant.

In Ref. [16] Sedrakian reported the results of a study aimed at clarifying the impact of SRC on neutrino emission in the aftermath of dUrca processes. Owing to the isospin dependence of nuclear forces, the correlated nucleon pairs discussed in Sec. 2.2.2 predominantly consist of a proton and a neutron, the momenta of which exceed the corresponding Fermi momenta. Electron scattering experiments have shown that in neutron-rich nuclei the deviation from the normal Fermi liquid momentum distribution is more pronounced for protons [54].

Within the approach proposed by Sedrakian, in which the neutrino emissivity is obtained from the one-loop approximation to the polarisation tensor of Eq. (33), the non Fermi liquid behaviour of protons and neutrons is taken into account by approximating the corresponding spectral functions—trivially related to the Green's functions through $P_N(k) = \text{Im}\, G_N(k)/\pi$—in the form

$$P_N(k) = Z_k \delta\big(k_0 - e_N(k)\big) + \frac{\Gamma_N}{\big[(k_0 - e_N(k)\big]^2 + \Gamma_N^2} + \dots \;, \qquad (36)$$

obtained by expanding about $\Gamma_N = 0$. Here, the δ-function term in the left-hand side corresponds to the quasiparticle approximation, whereas the second term takes into
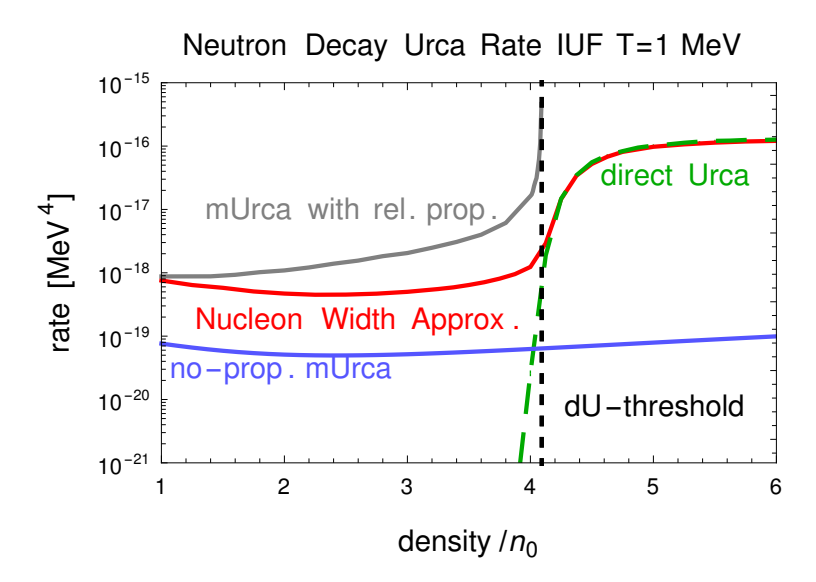
Fig. 10. Comparison between the density dependence of the neutron decay rate of Eq. (35), and the results obtained using different approximations; see text for details. Reprinted from Ref. [15] with permissions. © APS 2024. All rights reserved.

account the corrections arising at first order in the width Γ_N. Note that the leading contribution is corrected by the factor $Z_k < 1$, describing the reduced normalisation of the quasiparticle state due to SRC discussed in Sec 2.2.2. In view of the above considerations on the isospin dependence of correlations, the broadening correction to the neutron propagator has been neglected, setting $\Gamma_n = 0$. On the other hand, Γ_p has been estimated using the measured pn and pp scattering cross sections.

Figure 11, taken from Ref. [16], shows the dependence of the neutrino emissivity of npe matter on the proton fraction x_p, which is expected to drive the effect of SRC. The results of calculations performed using the spectra of Eq. (36)—normalised to those obtained from the FSA, Eq.(29)—are displayed for $T = 0.2$ and 1 MeV. The solid and dashed lines correspond to the full calculation and the quasiparticle approximation, respectively. For reference, the mUrca emissivity predicted by the model of Friman and Maxwell at $T = 1$ MeV is represented by the horizontal dot-dashed line.

The main conclusion emerging from Fig. 11 is that the finite quasiparticle lifetime significantly affects the dUrca emissivity. However, the interpretation of the observed results as correlation effects requires some qualifications. The appearance of high-momentum nucleons, providing unambiguous evidence of SRC, reveals the presence of correlated nucleon pairs in the nuclear matter ground-state, which cannot be taken into account by dressing the propagators appearing in Eq. (33)
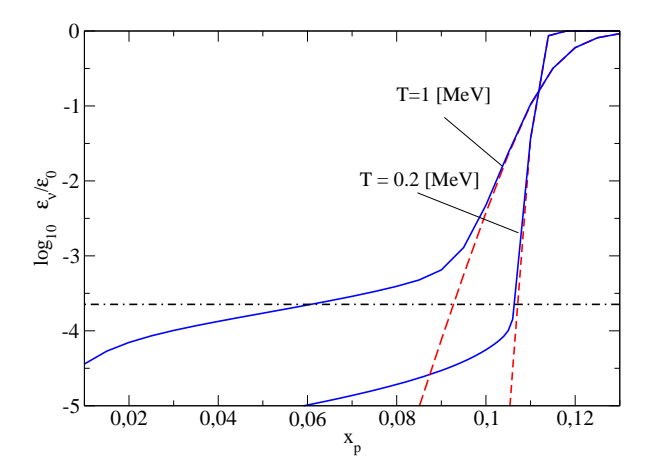
Fig. 11. Proton fraction dependence of the dUrca neutrino emissivity of *npe* matter, expressed in units of the corresponding FSA result. The solid and dashed lines correspond to the full calculation, performed using the spectra of Eq. (36), and to the quasiparticle approximation, respectively. For reference, the dot-dashed horizontal line shows the mUrca emissivity predicted by the model of Friman and Maxwell at $T = 1$ MeV. Reprinted from Ref. [16] with permissions. © APS 2024. All rights reserved.

and Fig. 9 (A). The results of a detailed analysis of correlation efffects in cold SNM—carried out by the authors of Ref. [55] using CBF perturbation theory and a realistic nuclear Hamiltonian—show that the high-momentum tail of the nucleon distribution originates from the admixture of a two-particle–two-hole component into the ground state. On the other hand, the contribution associated with self-energy insertions in the nucleon propagators only affects the normalisation of the quasiparticle states, Z_k, and turns out to be vanishing outside the Fermi sea.

4. Summary and outlook

In recent years, a number of theoretical studies [13–17] have exposed the limitations of the approximate treatment of neutrino emission from neutron stars matter proposed in the classic paper of Friman and Maxwell [11], and routinely employed by many authors afterwards [9]. Besides providing evidence that the assumption of full degeneracy—leading to the appearance of the activation threshold of the dUrca reaction—already fails at temperature as low as 1 MeV, the results of these analyses underscored the importance of taking into account more complex dynamical mechanisms, which lead to modifications the nucleon propagator. Moreover, they contributed to shed light on the connection between dUrca and mUrca processes, as well as on their role in determining the density dependence of the neutrino emission rate [15].

The treatment of thermal effects has been greatly improved by carrying out accurate phase space integrations [14]. It must be emphasised that the results of these

calculations are significantly affected by the temperature dependence of the proton and neutron energies and chemical potentials appearing in the corresponding Fermi-Dirac distributions. Moreover, all single-nucleon properties should in principle be obtained from the same model of nuclear dynamics employed to determine the equation of state and composition of matter. However, these issues, thoroughly discussed in Refs. [22] and [50], are largely disregarded in the literature.

Nucleon interactions have been widely treated within the oversimplified mean-field approach, which is conceptually inadequate to describe the mUrca processes. On the other hand, a number of studies performed using renormalised weak current opeators—defined in terms of correlated wave functions obtained from realistic nuclear Hamiltonians—have shown that the effects of correlations are, in fact, significant, and lead to a sizeable quenching of the weak transition amplitudes driving dUrca and mUrca processes alike [31, 36–38].

It should be noted that, because the renormalised weak operator acts on a single nucleon, it is quite natural to interpret the quenching of the corresponding transition matrix element in terms of a vertex correction, due to the renormalisation of the nucleon wave functions. The consistent inclusion of self-energy insertions in the nucleon propapagtor should be analyised using the formalism of Correlated Basis Function (CBF) perturbation theory, as discussed in Ref. [55] of the manuscript. Work in along this line is in progress, and the results will be reported in a forthcoming paper [18].

Correlation effects on the dUrca emissivity have been also studied using the one-loop approximation for the nuclear matter polarisation tensor [16]. However, the results of detailed calculations of the nucleon spectral functions and momentum distributions in cold SNM at equilibrium density, carried out using CBF perturbation theory and realistic nuclear Hamiltonians [56–58], show that the appearance of high-momentum nucleons, providing unambiguous evidence of correlated nucleon pairs, is associated with presence of a non-pole component in the nucleon Green's function. This contribution, which appears at lowest order of the CBF perturbative expansion, is not included in the model of Ref. [16].

Overall, the studies reviewed in this article, while being admittedly still limited by the lack of a consistent treatment of all quantities involved in numerical calculations, have provided valuable novel contributions, useful to shed light on the mechanisms of neutrino emission from dense and hot nuclear matter. Based on these recent achievements, the prospects for the development of a comprehensive and reliable theoretical framework, suitable for a fully quantitative characterisation of neutrino emissivity from neutron stars in the broad temperature and density region relevant to astronomical observations [19], appear to be promising. Attaining this goal will require the use of a microscopic model of nuclear interactions including both mean-field and correlation dynamics, as well as a consistent treatment of thermal effects on all nuclear matter properties at temperatures up to several tens of MeV. The approach based on non relativistic many-body theory and phenomenological nuclear Hamiltonians—which provides a quantitative description of

electron-nucleus scattering data revealing the occurrence of large density fluctuations due to NN correlations [59]—appears to have the potential to carry out this project.

Acknowledgements

References

1. A. Perego, S. Bernuzzi and D. Radice, *Eur. Phys. J. A* **55** (2019) 124.
2. A. Mezzacappa, E. Endeve, O. E. Bronson Messer and S. W. Bruenn, *Liv. Rev. Comput. Astrophys.* **6** (2020) 4.
3. M. Prakash, I. Bombaci, M. Prakash, P. J. Ellis, J. M. Lattimer and R. Knorren, *Phys. Rep.* **280** (1997) 1.
4. D. G. Yakovlev and C. J. Pethick, *Ann. Rev. Astron. Astrophys.* **42** (2004) 169.
5. L. Brandes, W. Weise and N. Kaiser, *Phys. Rev. D* **108** (2023) 094014.
6. L. Brandes and W. Weise, *Phys. Rev. D* **111** (2025) 034005.
7. R. W. Romani, D. Kandel, A. V. Filippenko, T. G. Brink and W. Zheng, *Astrophys. J. Lett.* **934** (2022) L17.
8. O. Benhar, *Particles* **6** (2023) 611.
9. D. Yakovlev, A. Kaminker, O. Gnedin and P. Haensel, *Phys. Rep.* **354** (2001) 1.
10. N. Chamel and P. Haensel, *Living Rev. Rel.* **11** (2008) 10.
11. B. L. Friman and O. V. Maxwell, *Astrophys. J.* **232** (1979) 541.
12. D. G. Yakovlev and K. P. Levenfish, *Astronomy & Astrophysics* **297** (1995) 717.
13. P. S. Shternin, M. Baldo and P. Haensel, *Phys. Lett. B* **786** (2018) 28.
14. L. Suleiman, M. Oertel and M. Mancini, *Phys. Rev. C* **108** (2023) 035803.
15. M. G. Alford, A. Haber and Z. Zhang, *Phys. Rev. C* **110** (2024) L052801.
16. A. Sedrakian, *Phys. Rev. Lett.* **133** (2024) 171401.
17. L. Tonetto, Thermal effects in nuclear matter and neutron stars, PhD thesis, Sapienza University of Rome (2024). https://iris.uniroma1.it/handle/11573/1715868.
18. L. Tonetto and O. Benhar, *Paper in preparation* (2025).
19. O. Benhar, A. Lovato, A. Maselli and F. Pannarale (eds.), *Nuclear Theory in the Age of Multimessenger Astronomy* (CRC Press, 2024).
20. O. Benhar and A. Lovato, *Phys. Rev. C* **96** (2017) 054301.
21. O. Benhar, A. Lovato and G. Camelio, *Astrophys. J.* **939** (2022) 52.
22. L. Tonetto and O. Benhar, *Phys. Rev. D* **106** (2022) 103020.
23. G. G. Raffelt, *Stars as laboratories for fundamental physics* (University of Chcago Press, 1996).
24. C. Hanhart, D. R. Phillips and S. Reddy, *Phys. Lett. B* **499** (2001) 9.
25. J. Carlson, S. Gandolfi, F. Pederiva, S. C. Pieper, R. Schiavilla, K. E. Schmidt and R. B. Wiringa, *Rev. Mod. Phys.* **87** (2015) 1067.
26. G. Baym and C. J. Pethick, *Landau Fermi-Liquid Theory* (John Wiley & Sons, 1991).
27. O. Benhar, *Nuclear Physics News* **26** (2016) 15.
28. O. Benhar, V. R. Pandharipande and S. C. Pieper, *Rev. Mod. Phys.* **65** (Jul 1993) 817.

29. J. Arrington, N. Fomin and A. Schmidt, *Annu. Rev. Nucl. Part. Sci.* **72** (2022) 307.
30. O. Benhar and S. Fantoni, *Nuclear Matter Theory* (CRC Press, 2020).
31. S. T. Cowell and V. R. Pandharipande, *Phys. Rev. C* **67** (2003) 035504.
32. J. W. Clark, *Progress in Particle and Nuclear Physics* **2** (1979) 89.
33. O. Benhar and M. Valli, *Phys. Rev. Lett.* **99** (2007) 232501.
34. O. Benhar, A. Polls, M. Valli and I. Vidana, *Phys. Rev. C* **81** (2010) 024305.
35. S. T. Cowell and V. R. Pandharipande, *Phys. Rev. C* **73** (2006) 025801.
36. O. Benhar and N. Farina, *Phys. Lett. B* **680** (2009) 305.
37. A. Lovato, C. Losa and O. Benhar, *Nucl. Phys. A* **901** (2013) 22.
38. A. Lovato, O. Benhar, S. Gandolfi and C. Losa, *Phys. Rev. C* **89** (2014) 025804.
39. A. Sedrakian and J. W. Clark, *Eur. Phys. J. A* **55** (2019) 167.
40. T. Takatsuka, R. Tamagaki and T. Tatsumi, *Progress of Theoretical Physics Supplement* **112** (1993) 67.
41. C. J. Pethick, *Rev. Mod. Phys.* **64** (1992) 1133.
42. T. Muto, T. Takatsuka, R. Tamagaki and T. Tatsumi, *Prog. Theor. Phys. Suppl.* **112** (1993) 221.
43. S. Tsuruta, M. A. Teter, T. Takatsuka, T. Tatsumi and R. Tamagaki, *Astrophys. J. Lett.* **571** (2002) L143.
44. G. Gamow and M. Schoenberg, *Phys. Rev.* **58** (1940) 1117.
45. G. Gamow, *My World Line: An Informal Autobiography* (The Vicking Press, 1970).
46. O. Benhar, *Structure and Dynamics of Compact Stars* (Springer, 2023).
47. R. Wiringa and S. Pieper, *Phys. Rev. Lett.* **89** (2002) 182501.
48. J. Carlson, V. R. Pandharipande and R. B. Wiringa, *Nucl. Phys. A* **401** (1983) 59.
49. B. S. Pudliner, V. R. Pandharipande, J. Carlson and R. B. Wiringa, *Phys. Rev. Lett.* **74** (1995) 4396.
50. O. Benhar, A. Lovato and L. Tonetto, *Universe* **9** (2023) 345.
51. R. B. Wiringa, V. G. J. Stoks and R. Schiavilla, *Phys. Rev. C* **51** (1995) 38.
52. F. J. Fattoyev, C. J. Horowitz, J. Piekarewicz and G. Shen, *Phys. Rev. C* **82** (2010) 055803.
53. A. Sedrakian and A. E. L. Dieperink, *Phys. Rev. D* **62** (2000) 083002.
54. O. Hen *et al.*, *Science* **346** (2014) 614.
55. O. Benhar, A. Fabrocini and S. Fantoni, *Phys. Rev. C* **41** (1990) R24.
56. S. Fantoni and V. Pandharipande, *Nucl. Phys. A* **427** (1984) 473.
57. O. Benhar, A. Fabrocini and S. Fantoni, *Nuclear Physics A* **505** (1989) 267.
58. O. Benhar, A. Fabrocini and S. Fantoni, *Nuclear Physics A* **550** (1992) 201.
59. O. Benhar, D. Day and I. Sick, *Rev. Mod. Phys.* **80** (2008) 189.